Measurement 163 (2020) 107946

Contents lists available at ScienceDirect

Measurement

journal homepage: www.elsevier.com/locate/measurement

Fluorescence detection of fluorescein and SYBR green-stained DNA by reflective cavity-coupled fluorometer – A quantitative study

Cheng-fu Chen

Department of Mechanical Engineering, University of Alaska Fairbanks, Fairbanks, AK 99775-5905, USA

ARTICLE INFO

Article history:
Received 13 December 2019
Received in revised form 15 March 2020
Accepted 7 May 2020
Available online 19 May 2020

Keywords:
Reflective cavity
Fluorescence detection
SYBR green
DNA
Fluorometer

ABSTRACT

With a miniaturized, reflective cavity-coupled fluorometer, a new fluorescence detection technique is presented with a quantitative analysis of its limits and sensitivity in detection. This paper is on a comparative study of fluorescence detection, on the same modularized fluorometer platform, to various combinations of light sources, optical filter lenses, reflectivity of the cavity wall, and fluorophore models. The quantitative comparison results allows for scrutinizing the mechanisms of noises in each measurement, including Raman scattering, and determining the limit of detection (LOD). This fluorometer enables detection of fluorescein at 0.4 nM and of SYBR Green (SG)-stained DNA at 0.05 ng μl^{-1} when equipped with a 450 nm laser diode, 550 nm cut-on longpass optical filter, and a polished reflective cavity. The detection of DNA can be further improved to a lower LOD by addressing the uncertainty in preparing the SG/DNA solutions with a consistent dye-base ratio throughout all the sample solutions.

1. Introduction

Detection of compounds with intrinsic or derivatized fluorescence [1] has been widely used to determine dissolved organic matter in aqueous environments [2], explosives [3], aerosol particles [4], and broken DNA strands [5]. It has also been used to probe photosynthetic activities [6], ethanol-involved metabolic activities [7], and fermentation processes [8]. In a typical laboratory setting with laser and high-sensitivity photo sensors, this technique is capable of detecting analytes at the parts-per-trillion level [9].

The fluorescence detection technique can be miniaturized for portable quantitative analysis, e.g., on microfluidic chips [5,9–12]. Often, miniaturization of fluorescence detection is concerned with acceptable detectability of fluorescence, because an even lower level of fluorescence emission in miniaturized devices is expected. Such weak fluorescence emission is attributed to the minute volume of the fluorophore solution held in miniaturized devices and the portable excitation light source for fluorescence emission. Solid-state lasers [9], laser diodes [10–12], or light emitting diodes (LEDs) [13,14] are preferred light sources because their compact size fits better to miniaturization. However, as opposed to lasers, these portable excitation sources produce less collimated and monochromatic light. For a less collimated light, only a fraction of its beams reaches the analytes. A less monochromatic light contains a smaller spectral radiance power to excite the fluorophores for fluorescence. Together these factors cause fluorophores to emit fluorescence at less intensity in miniaturized devices.

To improve the detectability of fluorescence, in miniaturized applications it typically acquires a delicate optical system capable of better focusing the excitation light on the fluorophore-laden cuvette for *brighter* excitation, and to guide the weak emission of fluorescence closer to the photo sensor for better detection. For instance, an enhanced fluorescence detection can be achieved by using a photodiode with better photocarrier collection efficiency. This was demonstrated in the detection of SG-stained DNA with a LOD at 0.9 ng μl^{-1} under a blue LED excitation [5]. On the other end, commercially available, miniaturized photo multiplier tubes are a popular option for the light sensor for on-chip detection [15]. Optical fibers can also be used to better guide the light of excitation closer to the fluorophore curvet as well as collecting the fluorescence at a proximal location next to the curvet [16,17].

Recently, a nontraditional approach to miniaturization of fluorescence detection was developed that better collects fluorescence emission for enhanced detection. This approach uses a reflective cavity to encapsulate the sample cuvette (flow cell) for fluorescence detection [18–21]. The idea is to confine the isotropic emission of fluorescence within the reflective cavity, allowing for continuous reflection until measurement is completed. This concept has been demonstrated with a spherical cavity 2 in. in diameter [18], a 1-inch dome-shaped reflector [22], a 2-cm diameter hemispherical reflector with $\rho > 0.9$ [19], and a silica-fused 2-inch-diameter column [20]. Each of these studies, albeit

E-mail address: cchen4@alaska.edu

https://doi.org/10.1016/j.measurement.2020.107946
0263-2241/

with a different excitation source, concluded that a reflective cavity can effectively enhance fluorescence detection. These achievements, however, are limited by their demonstration of feasibility under specific conditions.

Most recently the author demonstrated a battery-driven, portable fluorescence detector, which uses a reflective cavity (0.75 in. in diameter) to integrate a laser diode, an optical filter lens, and a cheap light sensor [21]. This detector enables a LOD of fluorescein at 0.4 nM with a 450 nm laser diode and 550 nm cut-on longpass filter. The design is simple and rugged, as it requires no delicate optical component except an optical filter lens. This current study further explores the instrumental response of the identified fluorometer to detection of fluorescein and SG-stained DNA with a wide span of hardware settings: three excitation sources (450 nm and 488 nm laser diodes and 453 nm LED), two optical filter lenses (532 nm bandpass and 550 nm cut-on longpass), and two cavities with different reflectivity (0.53 vs. 0.1). Using the same fluorometer platform with modularized configurations in different settings enables a comparative analysis, to explore the limits and sensitivity of detection and to explain the mechanisms of noises that arise in measurements.

2. Materials and methods

Fig. 1 shows a schematic of the fluorometer design, integrating a light source, flow cell (sample cuvette), optical filter lens, and a light sensor into a fluorescence detector. The sample solution flows through, or stays stagnant, in the flow cell for on-demand excitation. After excitation, the beams of fluorescence emission and excitation are retained concurrently within the reflective cavity for continuous reflection; part of the reflected excitation beams hit the flow cell for further fluorescence emission. The reflective cavity works somewhat like the "pumping cavity," a typical component in a laser used to scale up the number of photons.

Not shown in the schematic of Fig. 1 is an optical filter lens placed proximally to the hole labeled "next to light sensor." Any excitation light leaking through the filter will be picked up by the light sensor as background noise in the measurements. Therefore, the filter lens should be carefully selected to reduce the undesired spectra attributed to the excitation beams before it reaches the light sensor and the Raman scattering from the buffer solution.

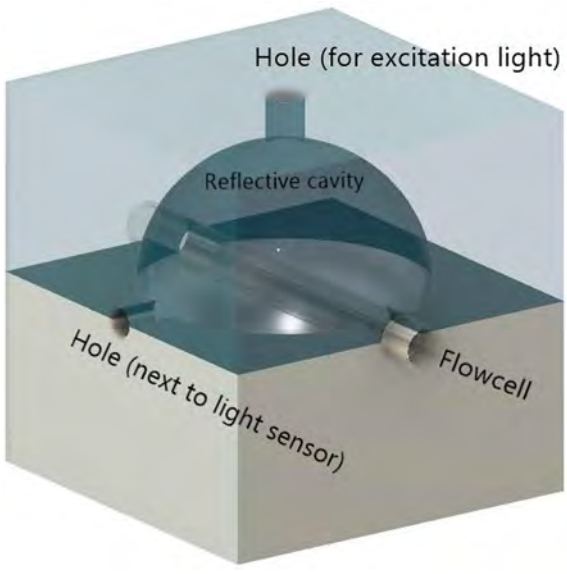

Fig. 1. Schematic of the fluorescence detector coupled with a reflective cavity.

Shown in Fig. 2 is an exploded view of the prototyped fluorescence detector. The reflective cavity was ball-milled, 0.75 in. in diameter, out of 304 stainless steel with a reflectivity $\rho = 0.53$at 450 nm after polish [23]. For comparison, a black cavity was also 3D-printed in testing. It was printed with black acrylonitrile butadiene styrene (ABS), a common 3D printing material with a reflectivity of about 0.1 [24]. The prototyping detail is available in Chen, Halford and Harmon [21]. In brief, a housing was fabricated to assemble the reflective cavity, flow cell, optical filter lens, and the laser diode. A few trials ensured that the laser diode was placed appropriately to focus its beam on the flow cell. Control of the power, light excitation, and the light sensor is managed by an Arduino board connected to a computer for data collection. The entire unit, once assembled, can be easily held in the palm of a hand.

Two fluorophore models, fluorescein and SG-stained DNA, were used to explore the instrumental response of the designed fluorometer. Fluorescein is the most widely used fluorescent dye for quantitative analysis. With a great quantum yield (about 0.8) and absorption and emission peaking at 493 nm and 513 nm, respectively, this safe dye can be readily tested once it is dissolved in water. In this work, the fluorescein solutions were prepared by a sequential dilution of a stock solution 1 mM of fluorescein in 0.5 L Milli-Q. A fluorescein-free Milli-Q was used as a blank solution of zero concentration.

SYBR Green is a popular fluorescent dye for detection of nucleic acids. Because of its unique binding modes to double-stranded DNA (dsDNA) [25], the SG-stained technique enables selective detection and quantification of DNA strands in gel electrophoresis, single-cell electrophoresis, and real-time PCR. The SG-DNA compound has absorption and emission spectra that peak at 498 nm and 522 nm, similar to those of fluorescein. Therefore, the SG-stained DNA was selected as a benchmark model for comparing the instrumental response to that of fluorescein. The SG-stained DNA solutions were prepared per the following procedure. First, the stain-free DNA solutions were diluted from a stock solution of Human Genomic DNA (Promega, Catalog No. G3041, Human Mixed, 223 μg/ml) with a Tris-acetate-EDTA (TAE) buffer (pH 8.0) to the designated concentrations. The SG solutions were diluted from the stock solution SYBR Green I nucleic acid gel stain (Sigma-Aldrich, CAS No. 163795–75-3, at a delivered stock concentration 10,000 × in DMSO) with DMSO at the 1:25 vol ratio. We added 1 μl of the diluted SYBR Green I solution to each prepared DNA solution. A DNA-free TAE buffer and DI water were individually used as a blank solution of zero concentration.

Laser diodes have a relatively narrowband spectrum of emission compared to LEDs. A laser diode and an LED with a close peak wavelength were selected to compare the influence of narrowband and broadband excitations on the emission of fluorescence. The laser diode selected for testing emits light at 450 nm, at which the emission diverges in a relatively narrowband spectrum, as characterized by its width at half maximum (FWHM) spectral width of 2 nm. The chosen LED has a peak wavelength of 453 nm and a relatively wide FWHM of 25 nm. The laser diode generates a radiant flux of 80 mW, as compared to 112–180 mW produced by the selected LED. Another laser diode, peaking at 488 nm, was also chosen for testing, for comparing the influence of the lasing wavelength on detection.

Two different optical filters were used individually to filter light from the reflective cavity for detection, a bandpass optical filter centered at 532 nm with a FWHM spectral width 10 ± 2 nm, and a longpass filter with a cut-on transmission wavelength at 550 nm.

A light sensor (TSL238-TCT-ND, Digi-Key) was selected for its wide range of responsivity, as shown in Fig. 3. Here the responsivity is defined as the ratio of the sensor's output signal to the sensor's incident irradiance, which is basically equivalent to the

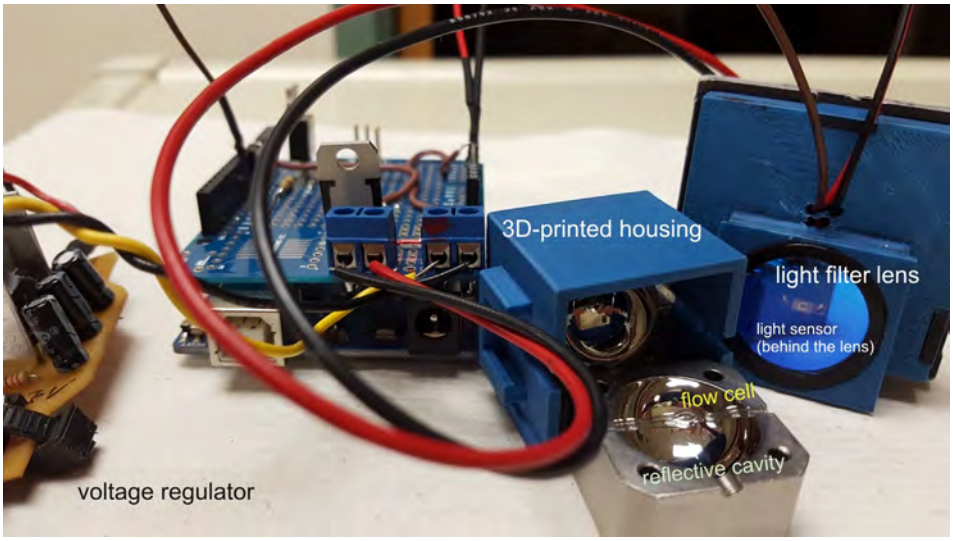

Fig. 2. A disassembled view of the prototype fluorescence detector. A polished reflective cavity was machined out of stainless steel to integrate the flow cell and excitation light. Both the excitation and fluorescence coexist and reflect in the reflective cavity, eliminating the need for placement and alignment of other optical components for detection.

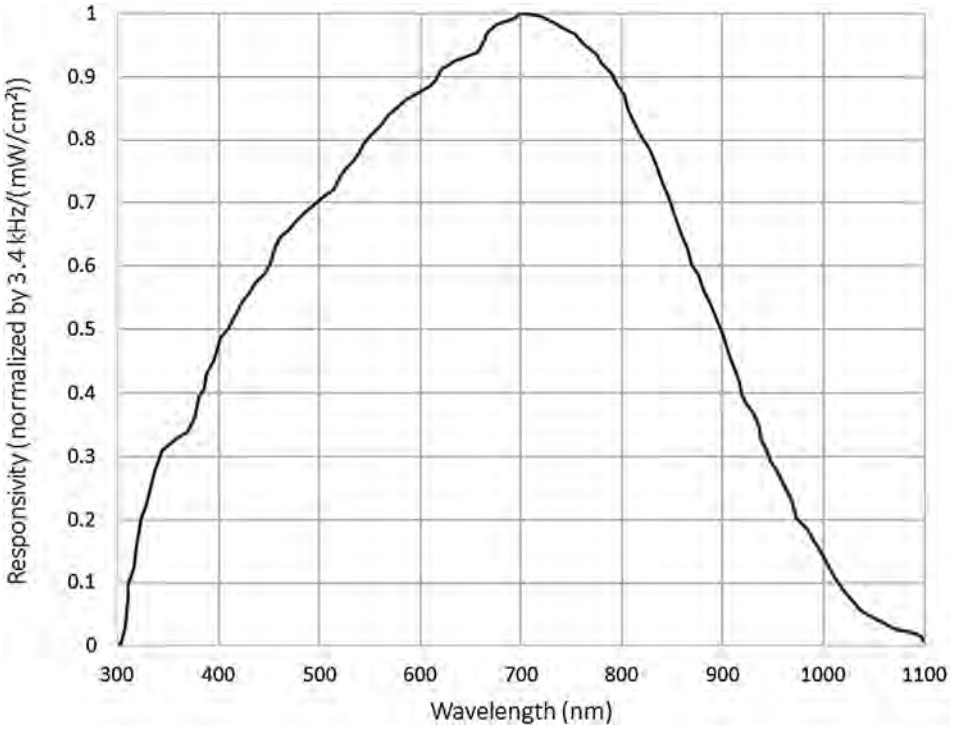

Fig. 3. Responsivity of light sensor TSL238-TCT-ND. (Reproduced from the specification sheet [26].)

so-called detection efficiency of a photo sensor. This light sensor reacts to fluorescence with a responsivity about 0.75. Because of its wide spectral responsivity, this sensor is also able to pick up the background noise, which is the spectral components of light at a wavelength other than fluorescence coexisting in the reflective cavity. In this work, the range 400–600 nm is of primary interest, as it covers the wavelengths of the excitation light, fluorescence, and the Raman scattering induced under the test conditions.

All measurements of fluorescence from fluorescein and SG-stained DNA were conducted at room temperature. Between each reading, we applied a customized cleaning protocol to clean the flow cell to remove any residual fluorophores. For testing fluorescein solutions, first a 10-second flow of DI water was sent through the flow cell, then we took a reading. We repeated these steps until the reading became consistent from one to another, indicating the light sensor's response to the fluorescein-free solution had reached a steady-state value, which represented the measured irradiance from the DI water. A few more readings of the steady-state value were collected, to determine their averaged value (y_{blank}) and three standard deviations ($3\sigma_{blank}$). For testing the SG-stained DNA solution, first the flow cell was cleaned with an alkaline detergent such as Windex. Then further cleaning involved drawing a Tris-Edta (TE) 1 $\times$ buffer solution through the flow cell and taking a reading; we repeated this step until the readings

become consistent, which served as the light sensor's response to the DNA-free buffer solution. Afterwards, a few more readings were collected to determine the averaged reading y_{blank} and the associated $3\sigma_{blank}$ as the background irradiance measured on the SG-DNA-free buffer.

For fluorophore-laden solution at a concentration, 25 repeated measurements were collected to determine the averaged value (y) and 3 standard deviations (3σ). The signal, S and noise, N were then calculated per [21]:

$$S = y - y_{blank} \tag{1}$$

$$N = \sqrt{(3\sigma)^2 + (3\sigma_{blank})^2} \tag{2}$$

The signal-to-noise (S/N) ratio is simply the value of dividing S by N. The LOD used in this paper is defined as the lowest concentration of a fluorophore-laden solution at which S/N is greater than one.

3. Results and discussions

3.1. Broadband LED excitation vs. Narrowband laser diode excitation

With the 453 nm LED and 450 nm laser diode, we compared the influence of narrowband and broadband excitations on fluorescein for the measured fluorescence irradiance and the noise. The measurements were conducted with the black cavity equipped with the 550 nm cut-on longpass optical filter and the light sensor discussed earlier.

The measured fluorescence irradiances are listed in Table 1 and plotted in Fig. 4. The data points are in a linear distribution for both the LED and the laser diode. The figure shows the LOD at 0.8 nM for the laser diode, and in the range of 4–8 nM for the LED. Using the calculated S/N ratio listed in Table 1 we can further determine an LOD of 4 nM for the LED excited fluorescence. The regression of the data points associated with the laser diode in Fig. 4 shows a more gradual slope, suggesting a more sensitive detection.

The comparisons suggest that an excitation source with a narrowband emission spectrum (e.g., laser diode) enhances the limit and sensitivity of detection. The comparisons are quantitative, because such comparative measurements were conducted on the same hardware platform with the laser diode and the LED which are closely matched in their specifications, except for the bandwidth in the excitation spectrum.

3.2. Optical filter lens: 532 nm bandpass vs. 550 nm cut-on longpass

Here we compare the detection results with the 532 nm bandpass and 550 cut-on longpass filters for a better understanding of their role in determining the S/N ratio and the sensitivity of detection. The measurements were conducted with the reflective cavity made of stainless steel equipped with the 450 nm laser diode and the light sensor. The results are also shown in Fig. 4 and listed in Table 1. The 550 nm filter enables a LOD of fluorescein at 0.4 nM with a more gradual slope in the data regression. With the 532 nm filter, the LOD is at 2 nM and the regression slope is about three times flatter. It is intriguing to note that the detection with the black cavity and 550 nm filter even enables a better LOD at 0.8 nM than the 2 nM achieved with the reflective cavity and 532 nm bandpass filter.

Why does the 532 bandpass filter perform worse than the 550 longpass filter in detection? One cause is that the 532 bandpass filter allows a higher intensity of the excitation light to pass through than the 550 longpass filter does, where it becomes part of the noise in detection. Recall that the emission of fluorescence and the excitation of light coexist in the designed reflective cavity, and both are transmitted through the optical filter lens to expose the light sensor. Keep this in mind, it can see that the transmission spectrum of the 532 bandpass filter in 522–542 nm, as compared to the 550 nm cut-on longpass filter, is closer to the emission spectrum of fluorescence (513 nm) as well as to the excitation spectrum of the light source (e.g., 450 nm for the laser diode, 453 nm for the LED). As such, the 532 nm bandpass filter allows a higher irradiance of both the fluorescence and excitation light to transmit for detection. The transmitted fluorescence yields the desired signal in the measurement, while the leaked excitation light contributes to an undesired noise which is larger than that with the 550 nm filter.

The other cause of poorer detection with the 532 nm filter is the Raman scattering effect. Raman scattering from the buffer solution adds noise to a measurement of fluorescence emission. Given the Raman shift of water in 3000–3700 cm^{-1} [27] and the incident photons at an energy of wavelength 450 nm, the photons of the Stokes scattering from H_2O molecules have a wavelength in the range 520–540 nm, as calculated per the well-known Raman shift equation. The Raman scattering thus occurs right in the spectral range of the 532 nm bandwidth filter. Typically, Raman scattering is ignorable as compared to fluorescence [28,29], but it will become relatively compatible in intensity to the weak emission of fluorescence from a fluorophore solution at a low concentration. Because the fluorescence and the light at other spectral wavelengths coexist and co-transmit through the optical filter to expose the light sensor for detection, it is critical in our design to prevent Raman scattering from illuminating the light sensor. This can be achieved by choosing an optical filter with a transmission spectrum outside the Raman scattering range. This design concept can be benchmarked with the calculated S/N ratios in Table 1. With the 532 bandpass filter lens and the reflective cavity, the LOD is 2 nM, at which S/N is 1.2. In the same hardware configuration but with a 550 nm longpass filter, the LOD is improved to 0.4 nM

Table 1
Measured irradiance (y) with the 3σ value (at the unit of μW/mm^2) and the calculated signal-to-noise ratio.

Concentration (nM) x	Black cavity LED 550 nm longpass filter		Black cavity laser diode 550 nm longpass filter		Reflective cavity Laser diode 532 nm bandpass filter		Reflective cavity Laser diode 550 nm longpass filter	
	$y \pm 3\sigma$	S/N	$y \pm 3\sigma$	S/N	$y \pm 3\sigma$	S/N	$y \pm 3\sigma$	S/N
0 (blank)	0.2766 ± 0.0074	–	0.2583 ± 0.0054	–	7.8353 ± 0.1060	–	1.2266 ± 0.0121	–
0.4	0.2817 ± 0.0087	0.4	0.2607 ± 0.0042	0.4	7.9286 ± 0.1000	0.6	1.3105 ± 0.0108	5.2
0.8	0.2806 ± 0.0068	0.4	0.2783 ± 0.0069	2.3	7.9663 ± 0.1074	0.9	1.3487 ± 0.0153	6.3
1	0.2800 ± 0.0074	0.3	0.2974 ± 0.0057	4.9	7.9878 ± 0.1128	1.0	1.3781 ± 0.0132	8.5
2	0.2830 ± 0.0074	0.6	0.3446 ± 0.0026	14.4	8.0121 ± 0.9961	1.2	1.4983 ± 0.0183	12.0
4	0.2936 ± 0.0075	1.3	0.4439 ± 0.0077	19.7	8.1302 ± 0.1058	2.0	1.8404 ± 0.0238	23.0
8	0.2963 ± 0.0073	1.9	0.5182 ± 0.0088	25.2	8.2383 ± 0.0902	3.1	2.1846 ± 0.0254	34.0
10	0.3094 ± 0.0071	3.2	0.7428 ± 0.0109	39.7	8.3612 ± 0.1163	3.3	2.8504 ± 0.0348	44.1
40	0.4279 ± 0.0084	13.5	2.3988 ± 0.0378	56.1	9.8898 ± 0.1442	11.5	8.6130 ± 0.1473	50.0

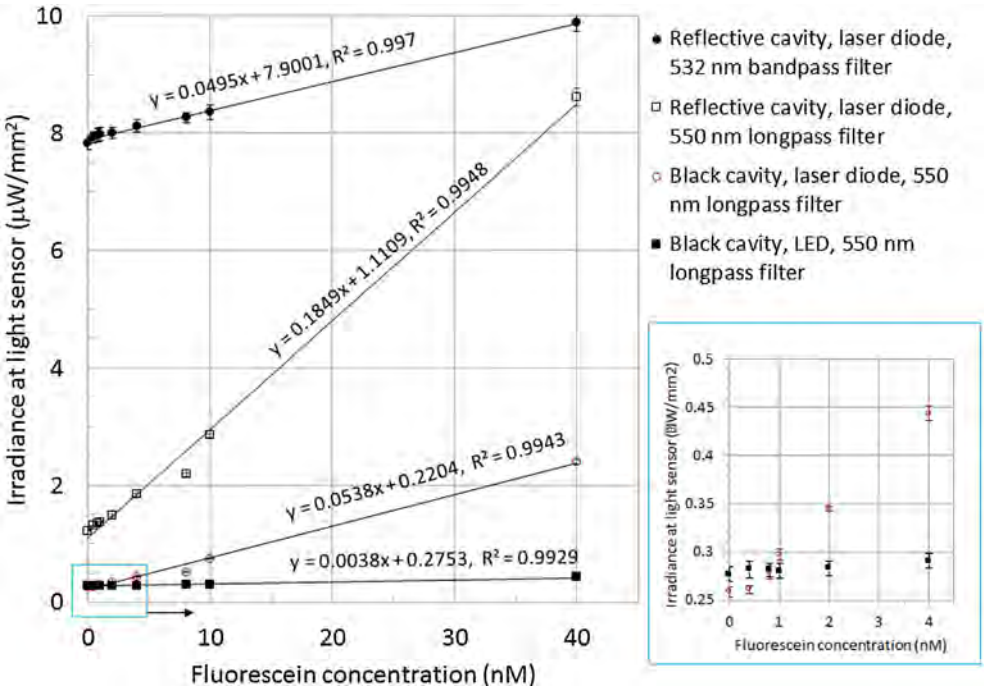

Fig. 4. Comparison of light source on measured irradiance of fluorescence emitted from fluorescein solutions of various concentrations. The bars indicate the 3σ range. (σ: one standard deviation.)

Table 2
Measured irradiance and the calculated S/N: 488 nm vs. 450 nm laser diode.

Concentration (nM) *x*	Reflective cavityLaser diode (488 nm) 550 nm longpass filter		Concentration (nM) *x*	Reflective cavity Laser diode (450 nm) 550 nm longpass filter	
	$y \pm 3\sigma$ (μW/mm²)	S/N		$y \pm 3\sigma$	S/N
0 (blank)	93.3167 ± 1.0670	–	0 (blank)	1.2266 ± 0.0121	–
0.5	95.4194 ± 1.0493	1.4	0.4	1.3105 ± 0.0108	5.2
1.5	97.4980 ± 0.9322	3.0	0.8	1.3487 ± 0.0153	6.3
2.5	99.5984 ± 0.9303	4.4	1	1.3781 ± 0.0132	8.5
3.5	103.1019 ± 1.0996	6.4	2	1.4983 ± 0.01825	12.0
4.5	106.9411 ± 1.1191	8.8	4	1.8404 ± 0.0238	23.0
5.5	110.6845 ± 1.0733	11.5	8	2.1846 ± 0.0254	34.0
6.5	114.7257 ± 1.0069	14.6	10	2.8504 ± 0.0348	44.1
			40	8.6130 ± 0.1473	50.0

with relatively small noise (S/N ratio 5.2). At the same concentration (0.4 nM), using the 532 nm bandpass filter shows more noise in detection (S/N ratio 0.6), implying that more non-fluorescence light passes the filter to activate the light sensor.

3.3. Laser diode 450 nm or laser diode 488 nm, which is better?

So far, the results show that the combination of the stainless steel reflective cavity coupled with a 450 nm laser diode and a 550 nm cut-on longpass filter lens provides the best LOD (0.4 nM of fluorescein) and sensitivity of detection *among* the measured. Can the LOD be further improved by using an excitation source that has a closer spectral match with the absorotion of fluorescein? This question is addressed by using the same hardware configuration but a 488 nm laser diode (GH04850B2G, 55 mW, DTR's Laser Shop), which has lasing wavelengths in 480–495 nm with peak excitation at 488 nm. In Table 2 and Fig. 5 below, we compare the fluorescence emitted from fluorescein excited individually by the 488 nm and 450 nm laser diodes. (Here the 450 nm data are from Table 1.)

The comparison shows that a larger irradiance of fluorescence, about two orders of magnitude more, was excited by the laser wavelength at 488 nm. It suggests that the excitation spectrum of the 488 nm diode in 480–495 nm, which more closely matches the absorption wavelength of fluorescein at 493 nm, promotes more intensive emission of fluorescence from the fluorophores.

The 3σ associated with the 488 nm laser diode are also about two orders of magnitude larger than that found with the 450 nm diode. Because the 3σ value indicates the magnitude of the noise produced in the fluorometer, a larger noise is also induced in the excitation of the 488 nm diode. The noise is attributed to use of an imperfect optical filter lens. The 550 nm longpass optical filter offers a theoretical cut-on wavelength of transmission at 550 nm, allowing light at a wavelength only longer than 550 nm to pass. Because the cut-on transmission is imperfect, a minute amount of light at a wavelength under 550 nm is allowed (leaked) through. The leaking light of excitation is the origin of the noise. The magnitude of a noise may be deliberated by a radiometric model (part of ongoing work toward design optimization): the total power of light passing an optical filter can be modeled as a spectral integral

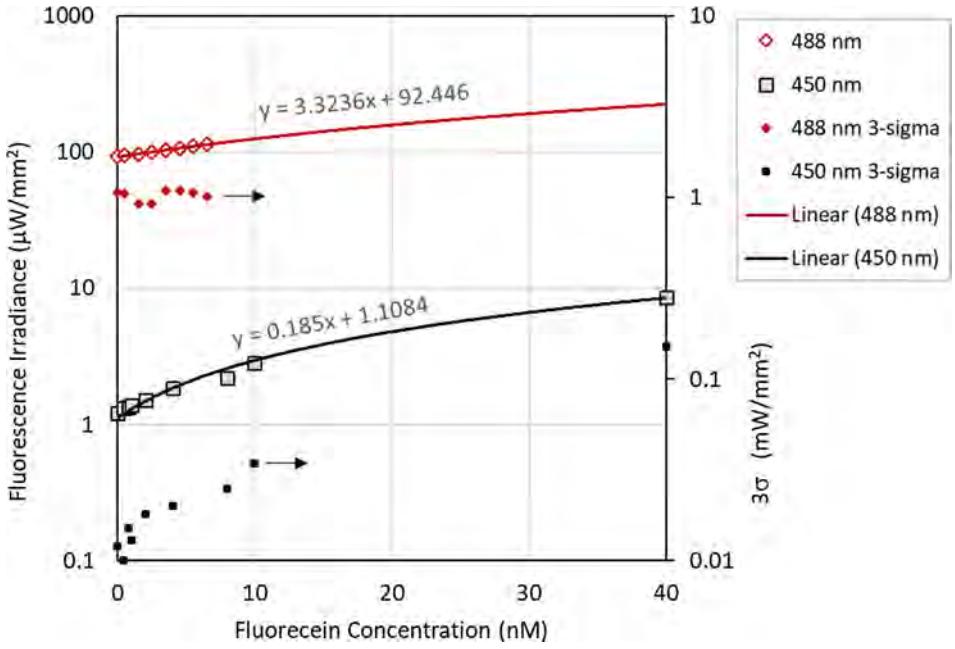

Fig. 5. Comparison of fluorescence emitted from fluorescein excited by lasing wavelength peaked at 488 nm and 450 nm, individually. 3σ values are at the scale on the secondary axis.

of the light spectrum and the transmission spectrum of the optical filter. Compared to the emission spectrum of the 450 nm diode in 448–452 nm, the emission spectrum of the 488 nm diode in 480–495 nm is closer to the cut-on threshold (550 nm) of the optical filter. Therefore, when the 488 nm laser diode is used, a larger amount of "leaking" light from the diode exposes the light sensor to yield a larger noise.

Using the 488 nm diode for excitation causes a gain both in the fluorescence emission and noise to the same order of magnitude. Together, both the gains compromise the S/N ratio, preventing the expected improvement in detection. With the S/N ratios listed in Table 2 one can see that the LOD 0.5 nM achieved by using the 488 nm laser diode is similar to the LOD 0.4 nM achieved by the 450 nm diode.

4. Detection of SYBR Green-stained DNA

4.1. Blind measurements and determination of LOD

The reflective cavity equipped with the 450 nm blue laser diode and 550 nm optical filter provides the best detection performance for our prototyped fluorometer, as concluded in the previous section. Because the SG-DNA compounds have a similar spectral property (absorption/emission at 497/520 nm) to those of fluorescein, this hardware configuration was used for measuring fluorescence from the SG-stained DNA solutions.

Blind measurements of 18 DNA-free or DNA-laden buffer solutions at various concentrations were conducted without a prior knowledge of the solution content. After the blind measurements were completed, each tested solution was then mapped to its pre-booked content. The results were then arranged in an increasing order of the measured signal (see Fig. 6). The prefix to each solution description is the order of a specific measurement taken. Each data point in the figure locates the averaged value of 25 repeated measurements with the 3σ error bars.

In this blind testing, the readings of the DNA-free solutions (DI water, TAE buffer, and TAE buffer with SG) spread in the 10–17 μW-mm^{-2} range, which serve as the blank readings y_{blank} (see Eq. (1)). The lowest reading, 10 μW-mm^{-2}, was yielded by DI water, which is about eight times larger than listed in Table 1. Such a significant difference is attributed to a few hardware-related factors. First, the beam of excitation from the laser diode is designed to aim at the center of the flow cell; in practice, any misaiming of the laser diode will affect the excitation efficiency because of its angle-dependent excitation intensity. Second, two flow cells were individually used in the measurements of the fluorescein and DNA solutions. Located in the middle of each flow cell is an oval-like, bulged volume (aka "bubble cell" hereafter), at which the laser diode was aimed to excite the specimen solution. The size and shape of the bubble cell differ slightly from one flow cell to another, although they were made by a skilled glass smith out of commercially available glass capillaries. The inconsistent geometry, however small, at the bubble cell yields an inconsistent radiant excitation energy delivered to the targeted specimen solution.

To further quantify the detection of DNA concentrations, the measured fluorescence of the SG-stained DNA solutions is extracted from Fig. 6 and separately plotted in Fig. 7. It shows that the data points are in a nonlinear distribution, in which the fluorescence begins to yield from the linear trend at the concentration 1 ng μl^{-1}. The yielding in fluorescence may be caused by the optical density effect, which is a yield of light between the densely distributed DNA molecules and/or fluorophores, per the Lambert law [30]. On the other end, the linear instrumental response can be visually determined in the concentration range up to 1 ng μl^{-1} (see Fig. 7).

The LOD of SG-stained DNA can be determined by the lowest concentration at which the measured fluorescence can be distinguished from that of the buffer solution. Given 17 μW-mm^{-2} as the largest reading from the buffer solution (see Fig. 6), the inset of Fig. 7 shows that one can visually determine the LOD as 0.05 ng μl^{-1}.

4.2. Raman scattering effect and uncertainty in preparation of the buffer

Raman scattering from the TAE buffer solution has insignificant influence on the measured fluorescence. EDTA in the TAE buffer

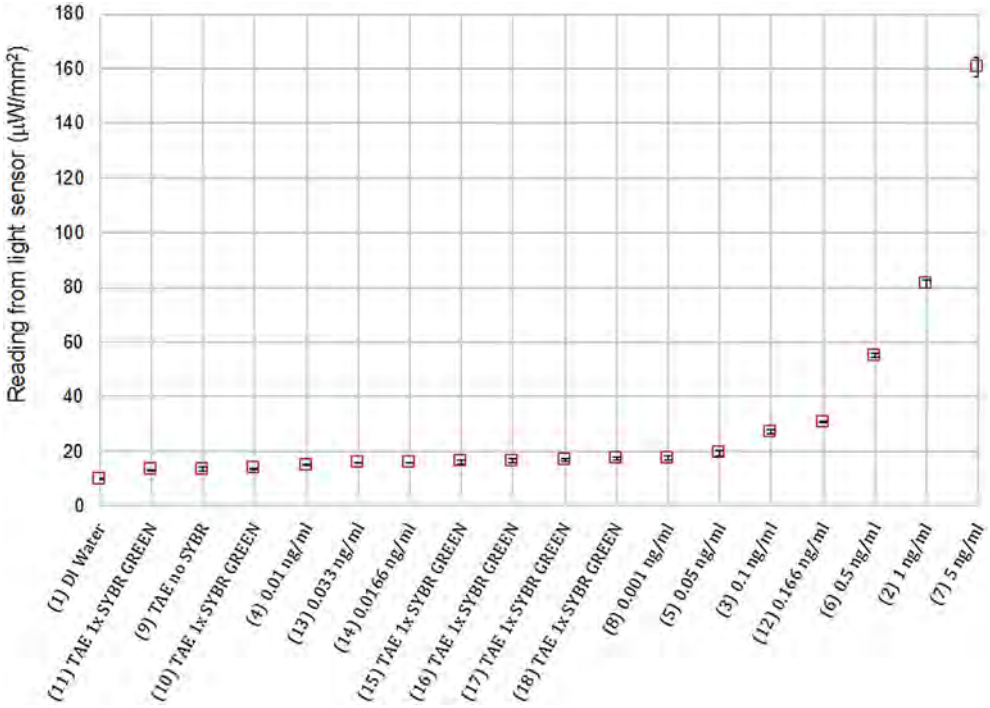

Fig. 6. Blind measurements of DNA-laden or DNA-free buffer solutions at an order prefix-labeled. Three DNA-free solutions: DI water, TAE buffer solution with or without SG.

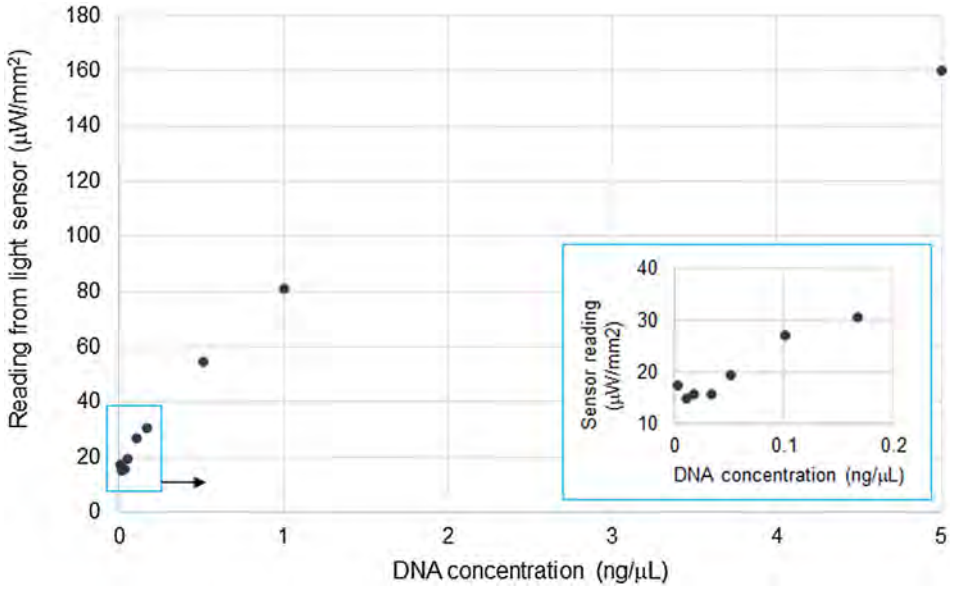

Fig. 7. Measured irradiance from SYBR green-stained DNA solutions. (For interpretation of the references to colour in this figure legend, the reader is referred to the web version of this article.)

has a strong Raman signal in 40–500 cm^{-1} [31], which yields Raman scattering in the wavelength range 450–460 nm when under excitation at the wavelength 450 nm as emitted by the blue laser diode. Most of the Raman scattering from the buffer solution is blocked out by the longpass filter which has a cut-on transmission spectrum at 550 nm.

Without considering the insignificant Raman scattering, each measured fluorescence of the SG-stained DNA solutions consists two parts of fluorescence irradiance. One is attributed to the SG-DNA compound, which is the desired fluorescence signal for interpreting the DNA concentration. The other part of the fluorescence *would* be from any non-bonded SG in the buffer solution, which is a noise that affects the detection. It is our surmise that non-bonded SG in the TAE buffer solution also emits fluorescence, which can be evidenced as follows. SG greatly increases its brightness (1000-fold) when bonded to DNA, as compared to the DNA-free [32]. This suggests that a DNA-free SG solution emits fluorescence but at a much weaker level. Our blind measurement results also suggest that non-bonding SG emits fluorescence – in Fig. 6, there is a notable increase in the measured fluorescence for the

SG-laden TAE buffer solution as compared to the SG-free TAE buffer. The only plausible explanation of this increase is due to the fluorescence emitted from SG in the buffer.

However, we are uncertain of the quantitative fluorescence from non-bonded SG. The uncertainty arises from our preparation for the SG-DNA solutions, in which whether the SG has overdosed the DNA is unknown. If so, there would be residuals of the non-bonded SG in the solution; if not, the measured fluorescence would underestimate the concentration of DNA because the non-bonded DNA does not fluoresce. Such an uncertainty in the measured fluorescence will be magnified in the detection of DNA at low concentrations, at which the intensities of the noise fluorescence and signal fluorescence are compatible and thus compromising the LOD.

4.3. Detection can be improved by fixing the uncertainty with a protocol for preparing SG-stained DNA solutions

A lower LOD would be achieved if this uncertainty can be resolved with a consistent protocol for preparing the SG-stained DNA solutions. To the author's knowledge, there is no protocol for dosing a concentration of DNA solution with SG to form the SG-DNA compounds in a consistent manner. SG interacts with DNA through surface binding, intercalation, and possibly precipitation, but the mechanisms are not well understood. Zipper et al. [25] measured the relative fluorescence intensity as a function of the dye/base pair ratio (dbpr). Their studies suggested that the relative fluorescence intensity remains constant in dbpr < 0.1 (under-dosing of dye) or dbpr greater than 10 (over-dosing of dye); but once dbpr is larger than 1000, the relative fluorescence intensity dramatically drops. Based on Zipper's findings, a protocol could be developed for a better and consistent preparation of the SG-DNA solutions that, hopefully, can lead to improved detection of fluorescence.

5. Conclusions

This work presented a quantitative comparison of fluorescence detection by a miniaturized reflective cavity-coupled fluorometer [21]. The use of a reflective cavity, 0.75-in. in diameter, distinguishes this work from the traditional techniques for fluorescence detection. The reflective cavity plays a multifaceted role in holding the sample solution, reflecting excitation light, and collecting fluorescence emission for detection, thus enabling a rugged and simple design without delicate optical systems (and their associated alignments) for high-sensitivity detection. All the measurements were conducted on the same fluorometer platform. This modularized platform allows for a quantitative comparison of the measured fluorescence in response to different light sources (LED vs laser diodes), optical filter lenses (532 nm bandpass vs. 550 nm cut-on longpass), reflectivity of the cavity wall (black vs. reflective), and fluorophore models (fluorescein vs. SG-stained DNA). The influence of each hardware component on detection and the mechanisms of noise arisen in each measurement, including Raman scattering, were discussed for determining the limit and sensitivity of detection. This fluorometer enables detection of fluorescein at 0.4 nM and of SG-stained DNA at 0.05 ng μl^{-1}, individually, when equipped with a narrowband 450 nm laser diode, 550 nm cut-on longpass optical filter, and a polished reflective cavity. The noise analysis of the measured DNA concentrations indicates that detection of SG-stained DNA may be improved with a better protocol for preparing the SG-stained DNA solutions with a consistent dye-base pair ratio.

CRediT authorship contribution statement

Cheng-fu Chen: Conceptualization, Methodology, Validation, Formal analysis, Investigation, Resources, Writing - original draft, Writing - review & editing, Visualization, Supervision, Project administration, Funding acquisition.

Declaration of Competing Interest

The authors declare that they have no known competing financial interests or personal relationships that could have appeared to influence the work reported in this paper.

Acknowledgements

This material is based in part upon work supported by the National Aeronautics and Space Administration (NASA) Grant Number NNX15AM63A. The author thanks J. Halford IV and D. Harmon for their assistance on prototyping and measurements, and A. Podlutsky for providing SYBR Green and DNA samples, and for his work with R. Williams for preparing the SYBR Green-stained DNA solutions for testing.

References

[1] S. Hapuarachchi, G.A. Janaway, C.A. Aspinwall, Capillary electrophoresis with a UV light-emitting diode source for chemical monitoring of native and derivatized fluorescent compounds, Electrophoresis 27 (20) (2006) 4052–4059.
[2] L. Patrolecco, N. Ademollo, P. Grenni, A. Tolomei, A. Barra Caracciolo, S. Capri, Simultaneous determination of human pharmaceuticals in water samples by solid phase extraction and HPLC with UV-fluorescence detection, Microchem. J. 107 (2013) 165–171.
[3] T. Caron et al., Ultra trace detection of explosives in air: Development of a portable fluorescent detector, Talanta 81 (1) (2010) 543–548.
[4] K. Davitt et al., 290 and 340 nm UV LED arrays for fluorescence detection from single airborne particles, Opt. Express 13 (23) (2005) 9548–9555.
[5] V. Namasivaya et al., Advances in on-chip photodetection for applications in miniaturized genetic analysis systems, J. Micromech. Microeng. 14 (1) (2004) 81.
[6] H.M. Kalaji et al., "Frequently asked questions about chlorophyll fluorescence, the sequel," (in eng), Photosynth. Res. 132 (1) (2017) 13–66.
[7] H. Kudo et al., A NADH-dependent fiber-optic biosensor for ethanol determination with a UV-LED excitation system, Sens. Actuat., B 141 (1) (2009) 20–25.
[8] F. Kensy, E. Zang, C. Faulhammer, R.-K. Tan, J. Büchs, Validation of a high-throughput fermentation system based on online monitoring of biomass and fluorescence in continuously shaken microtiter plates, Microb. Cell Fact. 8 (1) (2009) 31.
[9] J.R. Scherer, P. Liu, R.A. Mathies, Design and operation of a portable scanner for high performance microchip capillary array electrophoresis, Rev Sci Instrum 81 (11) (2010) 113105.
[10] R.F. Renzi et al., Hand-Held Microanalytical Instrument for Chip-Based Electrophoretic Separations of Proteins, Anal. Chem. 77 (2) (2005) 435–441.
[11] A.M. Skelley et al., Development and evaluation of a microdevice for amino acid biomarker detection and analysis on Mars, in: Proceedings of the National Academy of Sciences of the United States of America, 2005, pp. 1041–1046.
[12] X.-X. Fang, H.-Y. Li, P. Fang, J.-Z. Pan, Q. Fang, A handheld laser-induced fluorescence detector for multiple applications, Talanta 150 (2016) 135–141.
[13] J. Seo, L.P. Lee, Disposable integrated microfluidics with self-aligned planar microlenses, Sens. Actuat., B 99 (2–3) (2004) 615–622.
[14] A.I. Barbosa, P. Gehlot, K. Sidapra, A.D. Edwards, N.M. Reis, Portable smartphone quantitation of prostate specific antigen (PSA) in a fluoropolymer microfluidic device, Biosens. Bioelectron. 70 (2015) 5–14.
[15] G. Jiang, S. Attiya, G. Ocvirk, W.E. Lee, D.J. Harrison, Red diode laser induced fluorescence detection with a confocal microscope on a microchip for capillary electrophoresis, Biosens. Bioelectron. 14 (10) (2000) 861–869.
[16] S. Qi et al., Microfluidic devices fabricated in poly (methyl methacrylate) using hot-embossing with integrated sampling capillary and fiber optics for fluorescence detection, Lab Chip 2 (2) (2002) 88–95.
[17] J. Hübner, K.B. Mogensen, A.M. Jorgensen, P. Friis, P. Telleman, J.P. Kutter, Integrated optical measurement system for fluorescence spectroscopy in microfluidic channels, Rev. Sci. Instrum. 72 (1) (2001) 229–233.
[18] C. Monte, U. Resch-Genger, D. Pfeifer, D. Taubert, J. Hollandt, Linking fluorescence measurements to radiometric units, Metrologia 43 (2) (2006) S89.

[19] K. Kwon, B. Park, J. Shim, K. Yu, Fluorescence Detection System with Miniaturized Integrating Sphere, in: International Conference on Optical MEMS and Nanophotonics, 2011, pp. 235–236.
[20] J.N. Bixler et al., Ultrasensitive detection of waste products in water using fluorescence emission cavity-enhanced spectroscopy, in: Proceedings of the National Academy of Sciences, 2014, pp. 7208–7211.
[21] C.-F. Chen, J.H. Halford, D.M. Harmon, A sensitive portable fluorometer coupled with miniaturized integrating sphere, Meas. Sci. Technol. 31 (1) (2019) 015204.
[22] B. Park, K. Kwon, K. Yu, Non-imaging fluorescence detection system with hemispherical dome reflectors, in: International Conference on Optical MEMS and Nanophotonics, 2012, pp. 196–197.
[23] Mirrors and Etalons. Available: https://pe2bz.philpem.me.uk/Lights/-%20Laser/Info-999-LaserCourse/C06-M05-Mirrors+Etalons/mod06_05.htm.
[24] R.V. Morgan, R.S. Reid, A.M. Baker, B. Lucero, J.D. Bernardin, Emissivity Measurements of Additively Manufactured Materials, Los Alamos National LaboratoryLA-UR-17-20513, (2017).
[25] H. Zipper, H. Brunner, J. Bernhagen, F. Vitzthum, Investigations on DNA intercalation and surface binding by SYBR Green I, its structure determination and methodological implications, Nucl. Acids Res., 32 (12) (2004) e103-e103.
[26] TSL238 High-Sensitivity Light-to-Frequency Converter. Available: https://www.mouser.com/datasheet/2/588/TSL238_DS000157_2-00-948123.pdf.
[27] A.J. Lawaetz, C.A. Stedmon, Fluorescence intensity calibration using the Raman scatter peak of water, Appl. Spectrosc. 63 (8) (2009) 936–940.
[28] S. Nie, S.R. Emory, Probing single molecules and single nanoparticles by surface-enhanced Raman scattering, Science 275 (5303) (1997) 1102–1106.
[29] K. Kneipp, H. Kneipp, I. Itzkan, R.R. Dasari, M.S. Feld, Ultrasensitive chemical analysis by Raman spectroscopy, Chem. Rev. 99 (10) (1999) 2957–2976.
[30] P. Lambert, A literature review of portable fluorescence-based oil-in-water monitors, J. Hazard. Mater. 102 (1) (2003) 39–55.
[31] K. Krishnan, R.A. Plane, Raman spectra of ethylenediaminetetraacetic acid and its metal complexes, J. Am. Chem. Soc. 90 (12) (1968) 3195–3200.
[32] A. Dragan et al., SYBR Green I: fluorescence properties and interaction with DNA, J. Fluorescence 22 (4) (2012) 1189–1199.